# *In vivo* NMR microscopy allows short-term serial assessment of multiple skeletal implications of corticosteroid exposure

**Masaya Takahashi*, Felix W. Wehrli*†, Luna Hilaire*, Babette S. Zemel‡, and Scott N. Hwang***

*Department of Radiology, University of Pennsylvania Medical Center, 1 Silverstein, 3400 Spruce Street, Philadelphia, PA 19104; and ‡Division of Gastroenterology and Nutrition, The Children's Hospital of Philadelphia, 34th Street and Civic Center Boulevard, Philadelphia, PA 19104

Communicated by Britton Chance, University of Pennsylvania School of Medicine, Philadelphia, PA, January 23, 2002 (received for review May 5, 2001)

**Corticosteroids are in widespread clinical use but are known to have adverse skeletal side effects. Moreover, it is not known how soon these effects become apparent. Here, we describe a longitudinal approach to evaluate the short-term implications of excess corticosteroid exposure by quantitative *in vivo* magnetic resonance imaging and spectroscopy in conjunction with digital image processing and analysis in a rabbit model. Two-week treatment with dexamethasone induced a significant reduction in trabecular bone volume, which occurred at the expense of uniform trabecular thinning without affecting network architecture. Paralleling the loss in bone volume was conversion of hematopoietic to yellow marrow in the femoral metaphysis and atrophy of the femoral epiphyseal growth plate. This work demonstrates that detailed quantitative morphometric and physiological information can be obtained noninvasively at multiple skeletal locations. The method is likely to eventually replace invasive histomorphometry in that it obviates the need to sacrifice groups of animals at multiple time points. Finally, this work, which was performed on a clinical scanner, has implications for evaluating patients on high-dose steroid treatment.**

Bone loss and concomitant fractures of the vertebrae and hip are common clinical consequences of corticosteroid (CS) treatment for inflammatory conditions (1). The overall incidence of osteopenia induced by treatment with CS for a period of less than 6 months is approximately 50% (2). Further, excess CS causes conversion of hematopoietic to fatty bone marrow (3). Besides bone loss, CS treatment is known to have multiple other skeletal implications and thus represents a major public health problem. Of particular concern are pediatric patients treated with high doses of CS (4, 5). Little, however, is known about the early response to supraphysiologic CS levels on the musculoskeletal system.

Clinically, fracture risk is most commonly assessed on the basis of bone mineral density (BMD) measured with dual-energy x-ray bone absorptiometry (DEXA) or peripheral quantitative computed tomography (*p*-QCT). However, it is well known that BMD is not the sole determinant of bone strength and that architecture plays a significant role in conferring strength to the trabecular network (6–8). Unlike bone mineral densitometry, which affords a measure of global or regional bone density, we and others have shown that magnetic resonance microimaging ($\mu$-MRI) can quantify trabecular bone microarchitecture *in vitro* in specimens and biopsies (9–13) and *in vivo* in laboratory animals and humans (14–16). Whereas microcomputed tomography ($\mu$-CT) can generate high-resolution images of trabecular bone architecture (17), magnetic resonance (MR) is unique in that it is also able to provide detailed information on structure and function of soft tissues and bone marrow, which are also affected by steroid treatment.

One of the difficulties of imaging microarchitecture *in vivo* is achievement of sufficient resolution and signal-to-noise ratio to resolve individual trabeculae. Conventional MRI technology does not satisfy these more stringent requirements. To address the problems associated with the limited spatial resolution regime of *in vivo* $\mu$-MRI, image acquisition, restoration, and processing techniques have recently been developed in our laboratory (18, 19).

Here, we demonstrate the potential of serial combined $\mu$-MR imaging and spectroscopy for the quantitative assessment of short-term steroid exposure on trabecular bone, growth plate, and bone marrow composition in a rabbit model. The method, which was implemented on a standard 1.5-Tesla clinical MR scanner by using customized data acquisition and image processing techniques, is shown to provide detailed information on trabecular bone architecture and bone marrow changes occurring within a time span of 2 to 4 weeks of dexamethasone exposure.

## Materials and Methods

**Overall Study Design.** A preliminary series of experiments was designed to investigate the dose dependence of CS on trabecular bone volume (experiment I). The specific purpose of these experiments was to assess the magnitude of the response to CS exposure in terms of trabecular bone volume fraction and BMD measured by $\mu$-MRI and DEXA, respectively. These exploratory experiments then served to establish the dose and treatment period in the subsequent detailed studies (experiment II).

**Animal Protocol.** In experiment I, 20 male rabbits (3.5 to 4 month old, New Zealand White) were divided into three groups (a control and two treatment groups) immediately after baseline imaging by $\mu$-MRI and DEXA. The animals in the two treatment groups ($n$ = 7 and 6, respectively) were subcutaneously implanted with one or two pellets containing dexamethasone. The pellets are designed so as to ensure zero order kinetics, i.e., releasing the agent at a constant rate (Innovative Research of America, Sarasota, FL). One pellet provides a total of 35, mg/60 days, corresponding to daily dose of 0.2 mg/kg (i.e., 0.4 mg/kg for two pellets, respectively). Pellets were inserted through a small incision on the animal's neck. The animals in the control group ($n$ = 7) were sham operated. After the baseline scans, the imaging protocol was repeated at 4 and 8 weeks.

For *in vivo* imaging, the animals were anesthetized by intramuscular injection of ketamine/xylazine (3.5/5 mg/kg) supplemented by s.c. injection of urethane (0.2 g/kg). After the final imaging session, the animals in experiment II were euthanized with an overdose of anesthetic, and the left distal femur was excised and fixed in 70% ethanol for subsequent imaging by *p*-QCT and $\mu$-CT. The protocol of this study was approved by the Institutional Animal Care and Use Committee.

**Proton MR Imaging and Spectroscopy.** *In vivo* MR images of the femoral epiphysis for analysis of trabecular bone structure were

Abbreviations: CS, corticosteroid; BMD, bone mineral density; DEXA, dual-energy x-ray bone absorptiometry; *p*-QCT, peripheral quantitative computed tomography; $\mu$-MRI, magnetic resonance microimaging; $\mu$-CT, microcomputed tomography; TB/TV, trabecular bone volume/total volume; Tb.Th, trabecular thickness.

†To whom reprint requests should be addressed. E-mail: wehrli@oasis.rad.upenn.edu.

The publication costs of this article were defrayed in part by page charge payment. This article must therefore be hereby marked "*advertisement*" in accordance with 18 U.S.C. §1734 solely to indicate this fact.

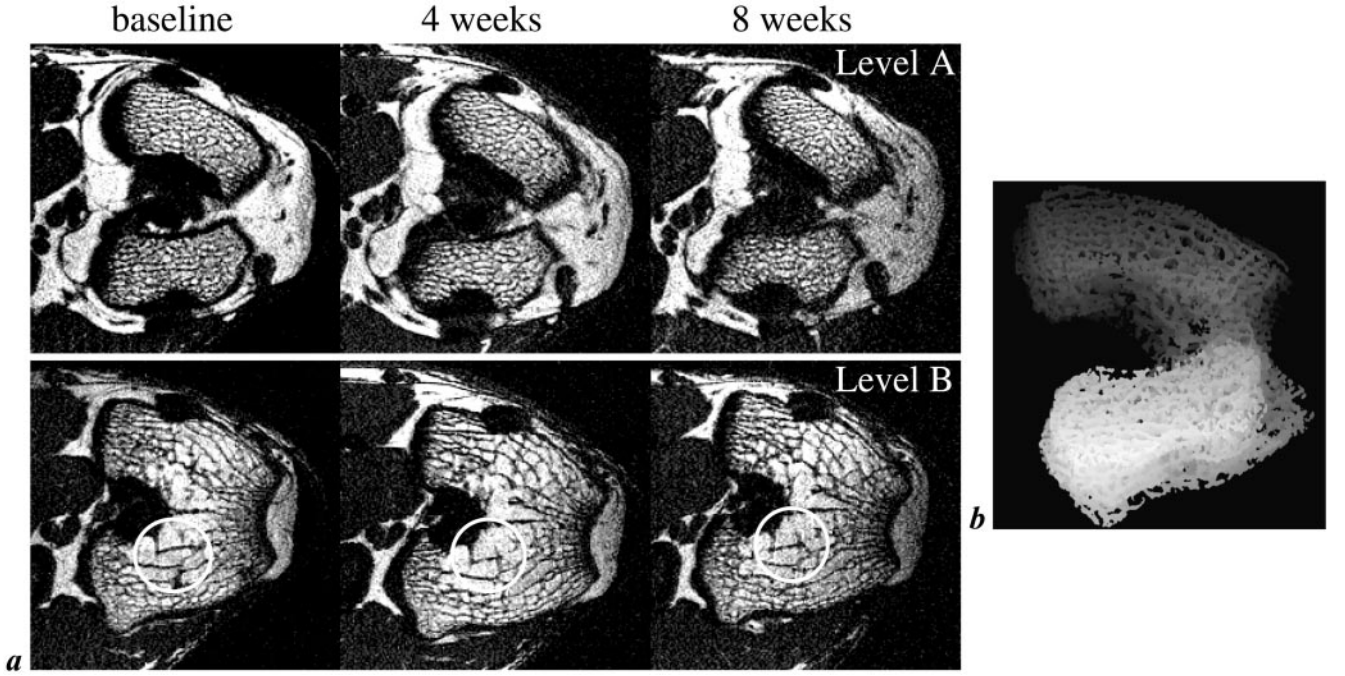


**Fig. 1.** Typical $\mu$-MR images of trabecular bone. (*a*) One of 28 contiguous transverse MR images perpendicular to the femoral shaft in the distal femur of the same rabbit at three different time points (image voxel size $98 \times 98 \times 300$ $\mu m^3$). Locations have been matched to allow comparison of the images collected at baseline and 4 and 8 weeks after s.c. implantation of dexamethasone pellets. Circles highlight structural features well reproduced in the repeat scans. Levels A and B represent locations ≈1 mm distal and 1.5 mm proximal to the intracondylar fossa. Note dense trabecular network in the distal epiphysis (Level A) but sparser trabeculation at the more proximal location (Level B). (*b*) Representative projection image of the distal femoral epiphysis of a live rabbit covering the volume analyzed. Projection direction is inferior to superior at an angle of 20° relative to the femoral anatomic axis.

obtained on a 1.5-Tesla whole-body imager (Signa, General Electric Medical Systems, Milwaukee, WI). The rabbits were positioned supine with a home-made Helmholtz coil tightly encompassing the left distal femur. For the purpose of reproducible positioning of the imaging region, a low-resolution coronal localizer scan was first performed from which the distal boundary of the high-resolution imaging volume was identified as the femoral condyle. Transverse images were subsequently acquired with a three-dimensional spin-echo pulse sequence (18) yielding contiguous images of $98 \times 98$ $\mu m^2$ pixel size and 300 $\mu$m slice thickness. All images were acquired at a pulse repetition time and echo time of 80 ms and 11 ms, respectively, and a radiofrequency pulse flip angle of 140°, in a total scan time of approximately 21 min. Image matrix size was $512 \times 512$ in experiment I and $256 \times 512$ in experiment II at a field of view of $50 \times 50$ $mm^2$ and $25 \times 50$ $mm^2$, respectively. Because the marrow in the epiphysis is predominantly fatty, the flip angle was selected so as to optimize the lipid signal. In experiment I, the scan volume comprised the epiphysis only (28 imaging slices) whereas in experiment II it comprised epiphysis, growth plate, and metaphysis (60 imaging slices).

Fig. 1*a* shows images from two different levels acquired in the same animal at three different time points. It is noted that bone appears with background intensity as a result of low proton density and short transverse relaxation times (9). The trabeculae are therefore visualized on the basis of the contrast with the bone marrow, which has high intensity because of the high concentration of protons in mobile lipids and water. The images demonstrate the positional reproducibility achievable in repeat scans. Examination of analysis parameters from multiple measurements in the same animal at a given time point afforded a reproducibility of 1.1% for bone volume fraction (coefficient of variation; data not shown). Fig. 1*b* represents a shaded surface display of the analysis volume comprising the distal femoral epiphysis (for details, see subsequent section *Image Processing and Analyses*).

Bone marrow composition was evaluated spectroscopically in axial sections in the epiphysis and metaphysis by using a spectroscopic imaging technique (20). Proton spectra were obtained in 13 min at a pixel resolution of $1.25 \times 1.25$ $mm^2$, a slice thickness of 4 mm, and digital spectral resolution of 5 Hz. For quantification, spectra from the epiphysis or metaphysis covering a $4 \times 4$-pixel region of interest were analyzed. Chemical shifts were referenced by setting the aliphatic methylene peak to 1.3 ppm at high frequency from (fictitious) tetramethylsilane. The peak areas in chemical shift regions 0–3.6 ppm (aliphatic fatty acid protons) and 3.7–7 ppm (olefinic fatty acid protons, glyceride protons, and water) were integrated, and, from the spectral integrals, a volume fraction of fat and water ($V_f$ and $V_w$) was calculated after correcting for partial saturation by using the algorithm described in ref. 20. The ratios $V_f/(V_f + V_w)$ and $V_w/(V_f + V_w)$ representing the relative volumes of fat and water were used as indices of the fractions of fatty and hematopoietic marrow, respectively.

**Bone Densitometry and $\mu$-CT.** BMD in $g/cm^2$ was measured (whole body and distal femur) by using the system's infant software option (QDR-2000, Hologic, Bedford, MA). The region of interest was positioned to encompass the femur and the distal subregion was coincident with the tip of the femoral condyle and comprised 5 mm so as to match the region assessed by $\mu$-MRI.

Volumetric trabecular BMD in $g/cm^3$ was obtained on the excised femurs by *p*-QCT (Stratec XCT 2000, Norland Medical Systems, Fort Atkinson, WI). The bone was scanned in a plastic tube, and the imaging slice was used for analysis selected on the basis of a longitudinal localizer image, from which a transverse image was obtained ($0.2 \times 0.2$ $mm^2$ pixel size and 2.3 mm slice thickness).

$\mu$-CT images were acquired on the femoral specimens on a

**Table 1. Effects of short-term CS exposure on skeletal parameters (absolute values) assessed by *in vivo* $\mu$-MR imaging and spectroscopy**

| | Control | | | Treated | | |
|---|---|---|---|---|---|---|
| | Baseline | 2 weeks | 4 weeks | Baseline | 2 weeks | 4 weeks |
| TB/TV, % | 23.3 ± 1.8 | 24.0 ± 2.2 | 25.1 ± 1.5 | 23.4 ± 1.1 | 22.2 ± 1.8 | 22.6 ± 1.2 |
| Tb.Th, $\mu$m | 103.9 ± 3.0 | 105.5 ± 1.5 | 108.4 ± 7.1 | 104.8 ± 1.1 | 98.5 ± 3.0 | 98.1 ± 2.8 |
| GP.Th, mm | 1.70 ± 0.41 | 1.50 ± 0.33 | 1.36 ± 0.24 | 1.32 ± 0.26 | 0.73 ± 0.09 | 0.64 ± 0.07 |
| Fat fraction, % | | | | | | |
| Epiphysis | 60.0 ± 2.7 | 62.5 ± 2.9 | 63.4 ± 1.9 | 61.2 ± 3.6 | 65.2 ± 2.5 | 67.7 ± 1.7 |
| Metaphysis | 46.2 ± 5.7 | 45.5 ± 11.7 | 49.4 ± 3.2 | 40.9 ± 7.9 | 56.1 ± 6.4 | 63.5 ± 2.7 |

TB/TV, trabecular bone volume fraction; Tb.Th, trabecular thickness; GP.Th, epiphyseal growth plate thickness.

$\mu$-CT scanner ($\mu$CT 80, Scanco Medical AG, Bassersdorf, Switzerland) for three slices spaced 2 mm apart at $35 \times 35 \times 35$ $\mu m^3$ voxel size. The three locations were chosen so as to correspond to the center and inferior and superior boundaries of the imaging volume used for *in vivo* $\mu$-MRI. Structural parameters (trabecular bone volume, trabecular thickness, bone perimeter, trabecular number, and trabecular separation) were calculated and averaged over all three slices by using the manufacturer's software.

**Image Processing and Analyses.** The $\mu$-MRI data from 16–18 slices (28 total, encompassing the epiphysis and excluding distal cortex and growth plate) were processed after manually isolating the trabecular bone area. From these data, the trabecular bone volume fraction TB/TV (trabecular bone volume/total volume) was computed pixel by pixel by using a histogram deconvolution algorithm, which removes image intensity nonuniformity and noise (19). The resulting images are maps of TB/TV in which the gray value represents the fractional occupancy of bone. A mean value of TB/TV was then determined for the entire trabecular volume of the epiphysis by pixel averaging across all slices. To derive trabecular thickness (Tb.Th) the $98 \times 98 \times 300$ $\mu m^3$ voxel TB/TV maps were subjected to subvoxel processing (21). Tb.Th was calculated for each cross section from the network length and TB/TV, and a global value was computed by averaging across all slices. In addition, coronal images were reconstructed from the 60 transverse images by reformation parallel to the femoral shaft for measuring the thickness of the epiphyseal growth plate (experiment II). The thickness was measured manually from a reformatted mid-line sagittal image by using NIH IMAGE (Version 1.61b7).

All parameters are expressed as mean ± SD and were tested by one-way ANOVA accounting for multiple comparisons (experiment I) or Student's *t* test (experiment II) by using commercially available statistics software (JMP, SAS Institute, Cary, NC) at each time point.

## Results

**Effect of Dexamethasone Dose on Trabecular Bone (Experiment I).** In the control animals, trabecular bone volume fraction (TB/TV) was found to increase from baseline throughout the protocol: 8.2 ± 4.5% at 4 weeks and 11.2 ± 5.9% at 8 weeks, respectively. TB/TV in the low-dose group (0.2 mg/kg, $n = 7$) decreased marginally by 3.9 ± 6.0% at 4 weeks and 0.6 ± 4.7% at 8 weeks whereas, in the high-dose group (0.4 mg/kg, $n = 6$), it declined 9.2 ± 4.9% at 4 weeks and 4.6 ± 3.5% at 8 weeks. The differences in change from baseline between treatment and control groups were significant in the low-dose group at 4 and 8 weeks ($P < 0.0005$ and $P < 0.001$), but the effect was greater in the high-dose group ($P < 0.00005$ and $P < 0.0001$). Whole-body BMD assessed by DEXA increased from baseline in the control group: 6.1 ± 1.9% at 4 weeks and 8.9 ± 2.4% at 8 weeks. In the low- and high-dose group, the increases from baseline at 4 and 8 weeks were 1.5 ± 2.8% ($P < 0.05$) and 4.7 ± 4.5%: (nonsignificant) and −2.2 ± 4.2% ($P < 0.0005$) and −4.2 ± 3.6% ($P < 0.00005$), respectively. Remarkably, however, there was no difference in regional BMD in the region of interest in the epiphysis matched to the $\mu$-MRI scan volume (data not shown).

**Short-Term Effects on Trabecular Structure, Growth Plate, and Bone Marrow (Experiment II).** The observed dose dependence of the decrease in trabecular bone volume fraction after 4 weeks of treatment guided experiment II, aimed at evaluating the earliest detectable treatment response. Accordingly, the time scale of dexamethasone exposure was compressed to 4 weeks, with measurements at baseline and at 2 and 4 weeks at a dose of 0.4 mg/kg. The two groups of animals studied (control and treatment, $n = 6$ each) were examined by $\mu$-MRI, DEXA, and proton spectroscopic imaging.

In the control group, $\mu$-MRI revealed growth in TB/TV of 3.3% at 2 weeks and 7.9% at 4 weeks, whereas the corresponding changes in the treatment group showed decreases of 5.0% at 2 weeks and of 3.3% at 4 weeks (Table 1 and Fig. 2*a*). These observations are commensurate with a significant treatment effect (expressed as the difference in change between the two groups; $P < 0.05$ and $P < 0.01$ at the two time points). To further investigate the structural ramifications of the observed bone volume changes, we processed the same *in vivo* $\mu$-MRI data to yield measures of Tb.Th, which in controls was found to increase 1.6% and 4.3% at 2 and 4 weeks, respectively. This trend was in substantial contrast to the one observed in the treatment group where thickness was found to decrease by 6.0% and 6.4% from baseline at corresponding time points ($P < 0.005$ and $P < 0.0001$; Table 1 and Fig. 2*b*). However, neither whole-body (Fig. 2*c*) nor regional (data not shown) DEXA detected significant differences between the two groups at any time points.

All treated animals demonstrated much faster age-related thinning of their epiphyseal growth plates than did the controls (Table 1 and Fig. 2 *d* and *e*). The control group growth plate thickness declined slightly compared with baseline (−10.1% at 2 weeks and −16.7% at 4 weeks) as would be expected during maturation. In contrast, the epiphyseal growth plate in the treated group diminished dramatically from its baseline value (−42.1%) within 2 weeks and was reduced further at 4 weeks (−50.3%; $P < 0.01$).

Bone marrow spectra obtained from the metaphysis (Fig. 3*a*) and epiphysis of the animals receiving dexamethasone indicated a conversion of hematopoietic to fatty marrow as evidenced by the reduction in $H_2O$ peak intensity. The marrow fat in the control group remained virtually constant during the first two weeks (−1.4% at 2 weeks, and +7.0% at 4 weeks). In comparison, in the treatment group, metaphyseal fat volume fraction increased substantially, +37.2% at 2 weeks and +55.3% at 4 weeks ($P < 0.05$ and $P < 0.01$; Table 1 and Fig. 3*b*). In the epiphysis, which has higher overall fat content (Table 1), the fat fraction increase in the treatment group was less prominent (+6.6% and +10.7% at 2 and 4 weeks, no significance).

To corroborate the *in vivo* findings, we further conducted ex-

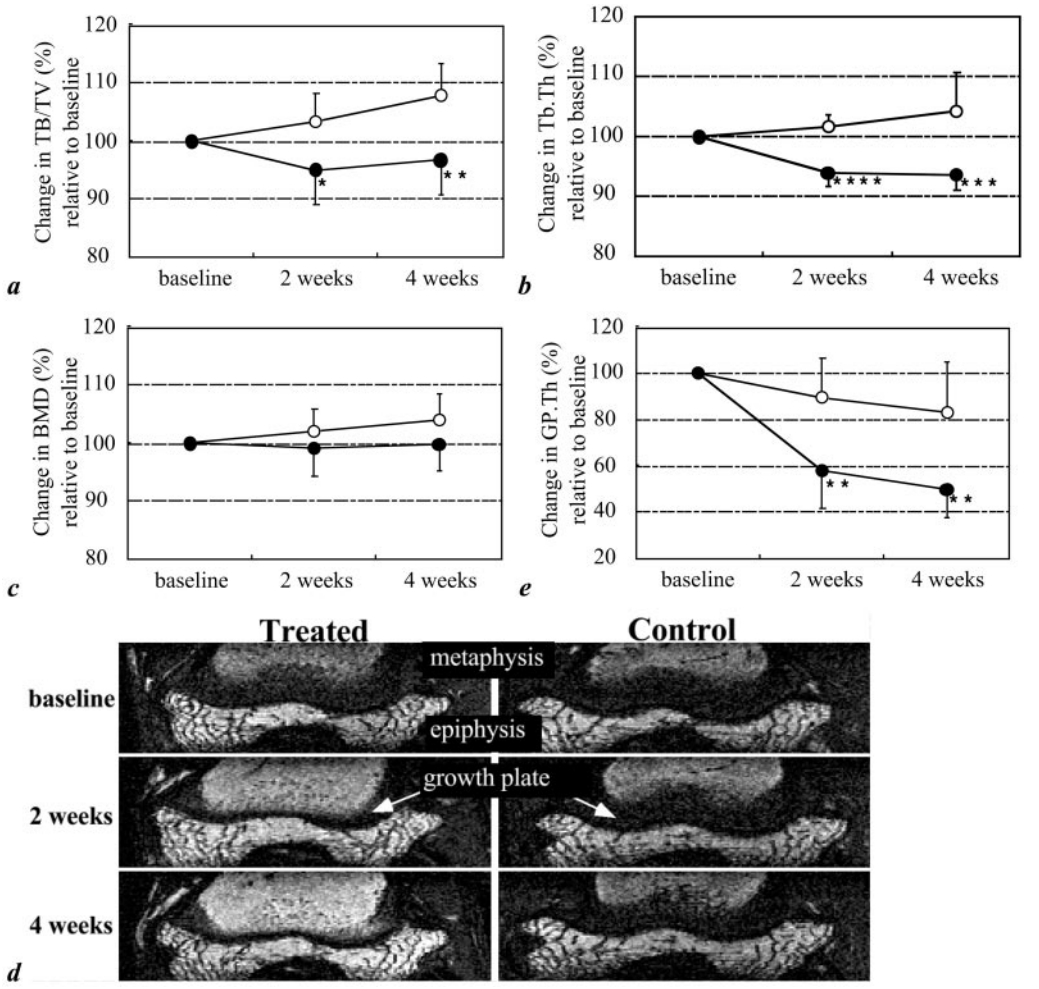


**Fig. 2.** Effect of dexamethasone on trabecular bone volume fraction (TB/TV) and trabecular thickness (Tb.Th) within 4 weeks of treatment, measured by $\mu$-MRI (open circle, control; filled circle, treated). (*a*) TB/TV. (*b*) Tb.Th. (*c*) Same as *a* for whole-body BMD obtained by DEXA (open circle, control; filled circle, treated). (*d*) Longitudinal images of the distal femur obtained by reformation of transverse MR images, with epiphyseal growth plate appearing as a dark band separating epiphysis and metaphysis, showing marked atrophy of epiphyseal growth plate thickness on MR reconstructed images in the treated animal. (*e*) Change in epiphyseal growth plate thickness (open circle, control; filled circle, treated). All data are expressed as percentage changes relative to baseline in each group (mean $\pm$ SD). *, $P < 0.05$; **, $P < 0.01$; ***, $P < 0.005$; and ****, $P < 0.0001$, treated compared with control, Student's unpaired, two-tailed *t* test.

periments on the excised distal femoral epiphysis by sacrificing six treated and six control animals after 4 weeks and examining the specimens by *p*-QCT and $\mu$-CT. Although the *p*-QCT data suggested a trend toward lower trabecular BMD in the treatment group ($0.415 \pm 0.028$ g/cm$^3$ vs. $0.395 \pm 0.033$ g/cm$^3$), this change was not significant. More revealing were the $\mu$-CT data, because they provide detailed structural information (Fig. 4 and Table 2). These data indicated a substantial reduction in TB/TV ($P < 0.05$) and Tb.Th ($P < 0.05$) but no difference in bone perimeter, trabecular number, and trabecular separation in the treated animals (Table 2), suggesting a mechanism involving uniform thinning.

## Discussion

The present *in vivo* longitudinal $\mu$-MR imaging and spectroscopy study on the distal femoral epiphysis in rabbits demonstrates that supraphysiological CS levels induce extraordinarily rapid trabecular bone loss in a dose-dependent manner. Only 2 weeks of CS exposure at a dose of 0.4 mg/kg caused substantial reduction in trabecular bone volume, unlike in the control animals whose bone volume fraction had increased during the same time period. The data provide strong evidence that bone atrophy occurs by uniform thinning rather than fenestration of trabecular plates. Further, 2 weeks of treatment resulted in dramatic thinning of the epiphyseal growth plate. Another hallmark of CS exposure was found to be the rapid conversion of hematopoietic to adipocytic marrow.

Although the literature is replete with clinical studies of CS-induced osteoporosis (22), investigations involving laboratory animals are relatively sparse. The rabbit model is particularly suited because bone loss in this animal is relatively fast (23, 24), which has been ascribed to the animal's mature skeleton, in which remodeling predominates over modeling (25). The rabbits used in the present study were 3.5–4 months old, at which age the femur has reached >95% of its adult length (26). Unlike in humans, the metaphysis was found to be devoid of trabeculae and thus was not studied except for the evaluation of the bone marrow, which in these young adult animals is predominantly hematopoietic at this location. Although the animals in the control group still showed growth in body weight, TB/TV, and BMD, dexamethasone either lowered these parameters or attenuated their increase. Bone loss occurred rapidly in the acute phase (within 2 weeks) but leveled off subsequently. We ascertained that the decreases in the rates of change were not due to loss in dexamethasone activity because the plasma levels of the agent were found to be constant throughout the treatment period (data not shown).

The rate of initial bone loss in humans is not known, but the clinical literature suggests that CS treatment results in substantial bone loss within 6 months in at least 50% of patients (1). In the rabbit, Grardel *et al.* (24) found substantially reduced total bone mass in animals receiving a daily dose of 0.7 mg/kg of prednisolone within 1 month. However, because the bioavailability of CS was different from that in our study (regarding both the compound used and its route of administration), the data are difficult to compare. In the current study, CS treatment of dexamethasone at a dose of 0.2–0.4 mg/kg showed multiple effects within 2 weeks. The major mechanism underlying CS-induced osteoporosis has been shown to be decreased osteoblast

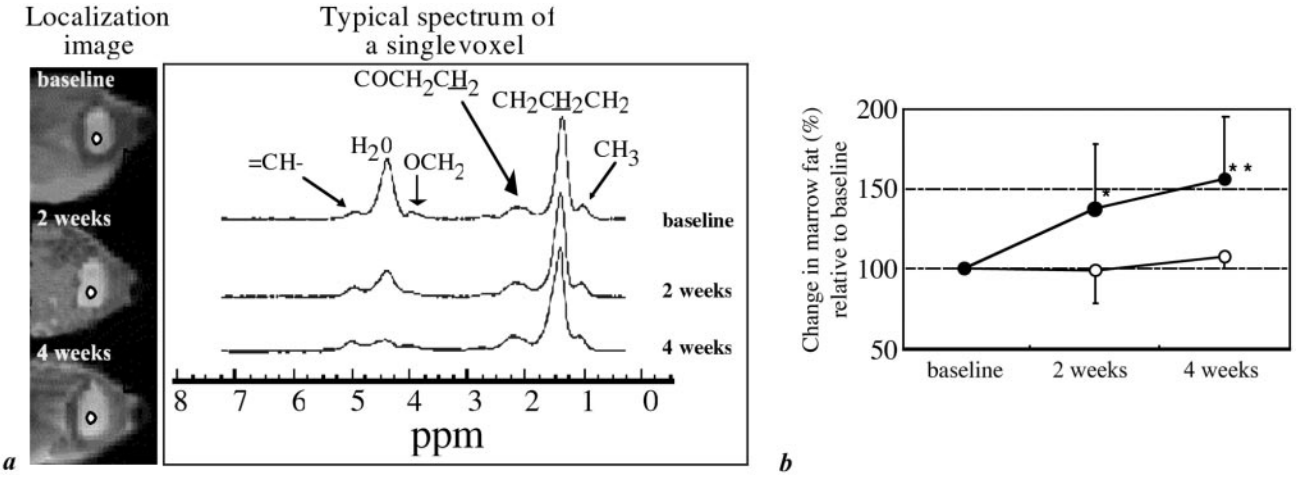


**Fig. 3.** Transverse localizer images indicating location of the bone marrow proton spectra (2 × 2 pixel region of interest) (*a*) in distal femoral metaphysis, obtained by spectroscopic imaging *in vivo* from the same animal at three time points. Spectra are from one of 64 × 64 spectroscopic imaging voxels (1.25 × 1.25 × 4 $mm^3$ voxel size). Spectral assignments correspond to water ($H_2O$) and triacylglyceride moieties. Peaks are referenced to fictitious tetramethylsilane (0 ppm). The reduced marrow cellularity (conversion of hematopoietic to fatty marrow) at 2 and 4 weeks on dexamethasone treatment is evidenced by the reduction in the intensity of the water signal. (*b*) Evolution of bone marrow composition in control and treated animals showing change from baseline. Data are expressed as changes relative to baseline in each group and represent mean ± SD. *, $P < 0.05$; **, $P < 0.01$, treated compared with control, Student's unpaired, two-tailed *t* test.

recruitment and impaired function, along with premature apoptosis (27), all leading to reduced bone formation. Additional contributing mechanisms involve suppression of intestinal calcium absorption and decreased renal tubular calcium reabsorption, along with increased urinary calcium excretion. It has also been suggested that the reduction in gonadal steroids caused by CS exposure may enhance resorption, thus leading to a dual effect of reduced formation and enhanced resorption (1). The combination of these effects could explain the extraordinarily rapid bone loss seen in our study.

The etiology of bone loss induced by gonadal steroid deficiency is well known, i.e., increased trabecular separation as a result of the resorption of entire trabecular elements. Unlike in estrogen or androgen deficiency, the architectural changes accompanying bone atrophy in CS-induced osteopenia are still controversial. Based on histomorphometry, Aaron *et al.* (28) describe the latter as characterized primarily by uniform trabecular thinning whereas Grardel *et al.* (24) found both thinner and fewer trabeculae. Chappard *et al.* (29) suggest that trabecular perforations typically do not occur as long as TB/TV is above a certain threshold. The close similarity of our *in vivo* $\mu$-MR image data obtained at different time points implies the network to be unaltered, at least during the early phase of bone loss, whereas trabecular thickness was significantly reduced. The *ex vivo* $\mu$-CT images that were obtained at much higher resolution than is achievable by *in vivo* $\mu$-MRI (35 $\mu$m vs. 98 $\mu$m, Table 1) corroborate such a hypothesis. The $\mu$-CT data show that 4 weeks of treatment does not lead to either increased trabecular separation or decreased trabecular number, which is commensurate with trabecular thinning. The results thus indicate that CS-induced bone loss occurs predominantly through trabecular thinning while keeping the trabecular network topology intact. This etiology may explain why fracture risk is rapidly reversed on cessation of steroid therapy (30). In contrast, osteoporosis caused by gonadal insufficiency is well known to lead to trabecular plate erosion that makes restoration of bone strength on regaining lost bone less likely.

Besides bone loss, CS treatment is known to adversely affect connective soft tissues, including skin and cartilage. Several mechanisms have been suggested to be involved in causing the effects of CS on the ephiphyseal growth plate. Chief among these is inhibition of chondrocyte proliferation (31, 32) and cartilage matrix production (33, 34), which result in growth suppression (5). CS treatment of children is well known to cause growth retardation (4). Therefore, assessment of growth plate development could be important as a means to predict the potential implications *o*f high-dose CS treatment of pediatric patients. Previous studies of the time-dependent effects of CS treatment on growth plate resorted to invasive procedures involving, for example, implantation of pins into the growth plate (35). MRI for assessing the growth plate was previously reported in a study involving sheep (36). Our study highlights the power of $\mu$-MRI to serially assess soft tissue implications of short-term exposure to excess CS by demonstrating the dramatic atrophy in epiphyseal growth plate after 2 weeks of treatment in small animals. Here, the same image data used for evaluating trabecular bone, through reformation of the high-resolution 3D images, allowed construction of longitudinal sections without the need for additional scans or repositioning of the animals.

Another important skeletal consequence of CS treatment is the conversion of hematopoietic to fatty marrow (37, 38). Such a transformation is consistent with CS inhibiting the differentiation of progenitor cells to hemopoietic cells (27). CS-induced hypertrophy and hyperplasia of marrow fat cells result in increased intraosseous pressure and a decrease in blood flow, which has been shown to lead to necrosis, fat embolism, microfracture, vasculitis, and intravascular coagulation (39). Localized spectroscopy is uniquely suited to monitor these changes *in vivo*

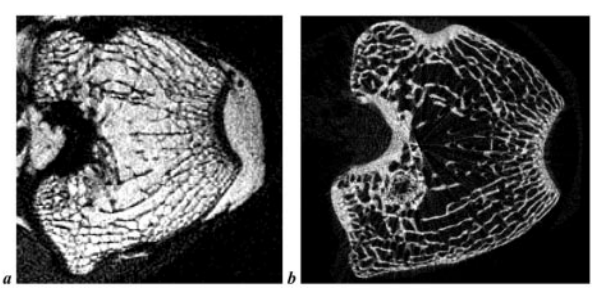


**Fig. 4.** Typical *in vivo* $\mu$-MR image (*a*, 98 × 98 × 300 $\mu m^3$ voxel size) and a slice-matched *ex vivo* $\mu$-CT image (*b*, 35 × 35 × 35 $\mu m^3$ voxel size) obtained from a treated animal showing excellent agreement.

**Table 2. Structural parameters of trabecular bone in distal femoral epiphysis measured by *ex vivo* $\mu$-CT**

| | T.Ar, mm$^2$ | B.Pm, mm | TB/TV, % | Tb.N., 1/mm | Tb.Th, $\mu$m | Tb.Sp, mm |
|---|---|---|---|---|---|---|
| Control ($n = 6$) | 120.6 ± 9.5 | 483.5 ± 37.3 | 32.8 ± 4.1 | 2.43 ± 0.11 | 134.9 ± 14.8 | 0.28 ± 0.03 |
| Treated ($n = 6$) | 118.7 ± 9.0 | 446.7 ± 16.0 | 28.0 ± 3.2 | 2.29 ± 0.19 | 114.9 ± 5.3 | 0.32 ± 0.04 |
| Significance | | | $P < 0.05$ | | $P < 0.05$ | |

T.Ar, Tissue area; B.Pm, bone perimeter; TB/TV, bone volume fraction; Tb.N, trabecular number; Tb.Th, trabecular thickness; Tb.Sp, trabecular separation.

because it can be practiced as part of the same overall measurement protocol. Here, we used a high-speed spectroscopic imaging technique that allows regional examination and quantification of bone marrow composition with high spatial resolution (20). Previous literature indicated increased fat fraction to be correlated with trabecular bone loss (37, 40), suggesting that fatty marrow takes the place of the lost trabecular volume. However, this interpretation is almost certainly incorrect because, in the present work, the greatest change in marrow composition is found in the metaphysis, which, in the rabbit, is almost devoid of trabeculation. Further, we found marrow conversion to continuously increase during the treatment whereas bone loss leveled off after 2 weeks, suggesting the two CS-induced effects on bone and bone marrow not to be directly related.

In summary, our study demonstrates the unique potential of $\mu$-MR imaging and spectroscopy in conjunction with digital image processing and analysis to investigate dynamic changes in trabecular bone structure, epiphyseal growth plate, and bone marrow composition longitudinally *in vivo*. The method has the potential for supplanting invasive histomorphometry, in that it allows following individual animals over time, therefore obviating the need to sacrifice animals at multiple time points. Finally, the methodology presented in this paper can easily be transferred to humans, for example, to follow pediatric patients undergoing high-dose steroid treatment.

We thank Dr. R. Kapadia for acquiring $\mu$-CT images. This work was supported by National Institutes of Health Grant RO1 45196.

1. Lukert, B. (1996) in *Osteoporosis*, eds. Marcus, R., Feldman, D. & Kelsey, J. (Academic, New York), pp. 801–820.
2. Gulko, P. S. & Mulloy, A. L. (1996) *Clin. Exp. Rheumatol.* **14,** 199–206.
3. Meunier, P., Aaron, J., Edouard, C. & Vignon, G. (1971) *Clin. Orthop.* **80,** 147–154.
4. Allen, D. B. (1996) *Endocrinol. Metab. Clin. North Am.* **25,** 699–717.
5. Alvarez, J., Balbin, M., Santos, F., Fernandez, M., Ferrando, S. & Lopez, J. M. (2000) *J. Bone Miner. Res.* **15,** 82–94.
6. Parfitt, A. M., Mathews, C. H., Villanueva, A. R., Kleerekoper, M., Frame, B. & Rao, D. S. (1983) *J. Clin. Invest.* **72,** 1396–1409.
7. Goldstein, S. A. (1987) *J. Biomech.* **20,** 1055–1061.
8. Hwang, S. N., Wehrli, F. W. & Williams, J. L. (1997) *Med. Phys.* **24,** 1255–1261.
9. Wehrli, F. W., Ford, J. C., Chung, H. W., Wehrli, S. L., Williams, J. L., Grimm, M. J., Kugelmass, S. D. & Jara, H. (1993) *Calcif. Tissue Int.* **53,** Suppl. 1, S162–S169.
10. Chung, H., Wehrli, F. W., Williams, J. L. & Kugelmass, S. D. (1993) *Proc. Natl. Acad. Sci. USA* **90,** 10250–10254.
11. Wehrli, F. W. (1995) in *Encyclopedia of Magnetic Resonance*, eds. Grant, D. M. & Harris, R. K. (Wiley, New York), pp. 4803–4811.
12. Majumdar, S., Newitt, D., Jergas, M., Gies, A., Chiu, E., Osman, D., Keltner, J., Keyak, J. & Genant, H. (1995) *Bone* **17,** 417–430.
13. Takahashi, M., Wehrli, F. W., Wehrli, S. L., Hwang, S. N., Lundy, M. W., Hartke, J. & Borah, B. (1999) *J. Bone Miner. Res.* **14,** 680–689.
14. Majumdar, S., Genant, H. K., Grampp, S., Newitt, D. C., Truong, V. H., Lin, J. C. & Mathur, A. (1997) *J. Bone Miner. Res.* **12,** 111–118.
15. Wehrli, F. W., Hwang, S. N., Ma, J., Song, H. K., Ford, J. C. & Haddad, J. G. (1998) *Radiology* **206,** 347–357.
16. Wehrli, F. W., Gomberg, B. R., Saha, P. K., Song, H. K., Hwang, S. N. & Snyder, P. J. (2001) *J. Bone Miner. Res.* **16,** 1520–1531.
17. Hildebrand, T., Laib, A., Muller, R., Dequeker, J. & Ruegsegger, P. (1999) *J. Bone Miner. Res.* **14,** 1167–1174.
18. Ma, J., Wehrli, F. W. & Song, H. K. (1996) *Magn. Reson. Med.* **35,** 903–910.
19. Hwang, S. N. & Wehrli, F. W. (1999) *Int. J. Im. Syst. Technol.* **10,** 186–198.
20. Hilaire, L., Wehrli, F. W. & Song, H. K. (2000) *Magn. Reson. Imaging* **18,** 777–786.
21. Hwang, S. N. & Wehrli, F. W. (2002) *Magn. Reson. Med.*, in press.
22. Lukert, B. P. & Raisz, L. G. (1990) *Ann. Int. Med.* **112,** 352–364.
23. Story, E. (1961) *Endocrinology* **68,** 533–542.
24. Grardel, B., Sutter, B., Flautre, B., Viguier, E., Lavaste, F. & Hardouin, P. (1994) *Osteoporos. Int.* **4,** 204–210.
25. Lindgren, J. U., DeLuca, H. F. & Mazess, R. B. (1984) *Calcif. Tissue Int.* **36,** 591–595.
26. Masoud, I., Shapiro, F., Kent, R. & Moses, A. (1986) *J. Orthop. Res.* **4,** 221–231.
27. Manolagas, S. C. & Weinstein, R. S. (1999) *J. Bone Miner. Res.* **14,** 1061–1066.
28. Aaron, J. E., Francis, R. M., Peacock, M. & Makins, N. B. (1989) *Clin. Orthop.* **243,** 294–305.
29. Chappard, D., Legrand, E., Basle, M. F., Fromont, P., Racineux, J. L., Rebel, A. & Audran, M. (1996) *J. Bone Miner. Res.* **11,** 676–685.
30. Van Staa, T. P., Leufkens, H. G., Abenhaim, L., Zhang, B. & Cooper, C. (2000) *J. Bone Miner. Res.* **15,** 993–1000.
31. Lewinson, D., Shenzer, P. & Hochberg, Z. (1993) *Calcif. Tissue Int.* **52,** 216–221.
32. Robson, H., Anderson, E., Eden, O. B., Isaksson, O. & Shalet, S. (1998) *J. Endocrinol.* **157,** 225–235.
33. Litchfield, T. M. & Sauer, G. R. (1996) *Connect. Tissue Res.* **35,** 189–195.
34. Sauer, G. R., Nie, D., Wu, L. N. & Wuthier, R. E. (1998) *J. Cell. Biochem.* **68,** 110–120.
35. Baron, J., Huang, Z., Oerter, K. E., Bacher, J. D. & Cutler, G. B., Jr. (1992) *Am. J. Physiol.* **263,** E489–E492.
36. Jaramillo, D., Connolly, S. A., Mulkern, R. V. & Shapiro, F. (1998) *Radiology* **207,** 637–645.
37. Warman, M. & Boskey, A. L. (1983) *Metab. Bone Dis. Rel. Res.* **4,** 319–324.
38. Vande Berg, B. C., Malghem, J., Lecouvet, F. E., Devogelaer, J. P., Maldague, B. & Houssiau, F. A. (1999) *Arthritis Rheum.* **42,** 1405–1411.
39. Cui, Q., Wang, G. J. & Balian, G. (1997) *J. Bone Joint Surg. Am.* **79,** 1054–1063.
40. Martin, R. B. & Zissimos, S. L. (1991) *Bone* **12,** 123–131.